ASTM INTERNATIONAL

Journal of
Testing and Evaluation

Jinghao Li,[1,2] John F. Hunt,[3] Shaoqin Gong,[1] and Zhiyong Cai[2]

DOI: 10.1520/JTE20140270

Testing and Evaluation of a Slot and Tab Construction Technique for Light-Weight Wood-Fiber-Based Structural Panels Under Bending

Journal of Testing and Evaluation

doi:10.1520/JTE20140270 available online at www.astm.org

Jinghao Li,[1,2] John F. Hunt,[3] Shaoqin Gong,[1] and Zhiyong Cai[2]

Testing and Evaluation of a Slot and Tab Construction Technique for Light-Weight Wood-Fiber-Based Structural Panels Under Bending

Reference

Li, Jinghao, Hunt, John F., Gong, Shaoqin, and Cai, Zhiyong, "Testing and Evaluation of a Slot and Tab Construction Technique for Light-Weight Wood-Fiber-Based Structural Panels Under Bending," *Journal of Testing and Evaluation* doi:10.1520/JTE20140270. ISSN 0090-3973

Manuscript received June 23, 2014; accepted for publication April 8, 2015; published online August 21, 2015.

[1] Department of Biomedical Engineering, Wisconsin Institutes for Discovery, and Materials Science and Program, University of Wisconsin-Madison, Madison, WI 53715.

[2] USDA Forest Service, Forest Products Laboratory, Madison, WI 53726.

[3] USDA Forest Service, Forest Products Laboratory, Madison, WI 53726 (Corresponding author), e-mail: jfhunt@fs.fed.us

ABSTRACT

This paper presented construction and strain distributions for light-weight wood-fiber-based structural panels with tri-grid core made from phenolic impregnated laminated paper composites under bending. A new fastening configuration of slots in the faces and tabs on the core was applied to the face/core interfaces of the sandwich panel in addition to epoxy resin. Both normal strain gages and shear strain gages were attached on these panels to analyze inside strain distributions by third point load bending test. The purpose of the bending test was to investigate the various strain distributions of panels with different face/core configurations that identified the critical failure modes for future design. In this research, four panels with different configurations were constructed to analyze the influence of strain distributions for bending behavior. Either maximum localized normal strain or shear strain were used to judge failures and associated failure modes through observation. Test results of strain distribution showed normal strain was primarily carried by both top and bottom faces. As bending load increased, compression buckling occurred on the top surface of some panels with thinner faces. Face thickness and stiffness significantly affected the strength of the panel as evident by nonlinear strain behavior. Meanwhile, the shear strain was primarily taken by the ribs in the structural core, and shear failure always occurred in the longitudinal linear ribs of core with thicker faces. The shear strain in the cross ribs was approximately half that of the longitudinal linear ribs in the same section of shear zone, which was consistent with the geometric formula. The problem of panel imperfections resulting in either face compression buckling or rib shear buckling could be overcome by further design optimization, and the analytical modeling for bending design and evaluation was presented.

Keywords

sandwich panel, tri-grid core, wood-fiber-based laminated paper, tab and slot configuration, strain gage, strain distribution, bending testing, failure mode

Introduction

Sandwich composite construction is generally used where the strength-to-weight ratio is the predominant design criterion. Usually the panels are composed of a low density core and stiff and strong faces. Sandwich composite structural panels are used for a wide range of applications including aircraft, ships, buildings, infrastructure, transportation, furniture, and packaging [1–5]. However, each specific application dictates different performance requirements, and thus, there is a need to provide flexible structural design for both core and faces to meet these requirements. Several types of traditional structural core such as foam core, honeycomb core, corrugated core, or truss core have been widely used in sandwich composites. They are typically sandwiched between two face layers made from fiber-reinforced polymers (FRP) or other stiff metals. Allen et al. conducted early investigations on the fundamental mechanical models of structural panels and reported the mechanical behaviors of sandwich structures with a honeycomb core [6]. During the last several decades, a number of researchers have explored multi-functional lattice structures characterized by mechanical performance, efficient energy dissipation, and wave absorption [7–9]. For instance, Evans et al. showed that lattice cores not only lead to lower density than traditional solid materials but also produce better mechanical performance compared with that of honeycomb or foam cores at the same cost [10]. Chen and Tsai established an integrated equivalent stiffness model on the static behavior of lattice grid structures with or without faces [11]. Fan et al. demonstrated the advanced mechanical performance of lattice sandwich panels under static mechanical testing [12]. Several manufacturing approaches have been proposed to fabricate these lattice structures using variable materials and for various applications [13,14]. Han et al. introduced a typical manufacturing process for an interlocked composite lattice grid arrangement that could offer improved performance for some applications [15]. However, most of these sandwich structures reported were made from metal or FRP rather than renewable materials such as wood fiber or paper. As the demand for sustainability increases, there is a unique challenge and opportunity to develop green composites as lightweight materials for a wide range of applications. These wood-fiber-based composite materials from renewable forests with various performance based on the flexible design could be used in tactical shelters, air pallets, packaging, building materials, transportation, and etc.

Our aim is to develop high-performance engineered structural panels using a significant portion of wood-fiber-based composite materials. Previously, we reported on a wood-fiber-based structure panel made of high-performance and water-resistant phenolic impregnated laminated paper [2,16]. A stiff, interlocking tri-axial core structure was developed for these composites assembled as a linear continuous rib double-slotted at 1/3 the width or single-slotted at 2/3 the width of the rib. As shown in **Fig. 1**, the double-notched ribs were used in the main rib orientation, and the 2/3 notched ribs were inserted from either the top or bottom side to create a tri-grid core structure that bonded both top and bottom laminated paper faces with epoxy resin. The initial static mechanical testing showed that the quality of adhesive interfaces between the core and the faces significantly affected the panel stability. Premature peeling at the face and core interface of the panels is an unacceptable failure mode for engineering applications. Therefore, it is essential to improve the shear transfer capacity of the face and core interface of the panel.

A new fastening configuration with slots in the faces and tabs on the ribs was developed and investigated as an approach to reduce failure caused by the initial weak adhesive interface between the face and core of the panel (**Fig. 2**). The goal was to increase shear transfer to the core through this tab/slot configuration. This paper reports the construction of sandwich composite structural panels with a fastening configuration and the distribution of both normal and shear strains inside of each panel with four different configurations using a third point load bending test.

Material Properties

The mechanical properties of the materials used for fabricating the wood-fiber-based sandwich composite structural panels were obtained by in-house material testing according to ASTM

FIG. 1 Fabrication of tri-axial core structure using linear material [2].

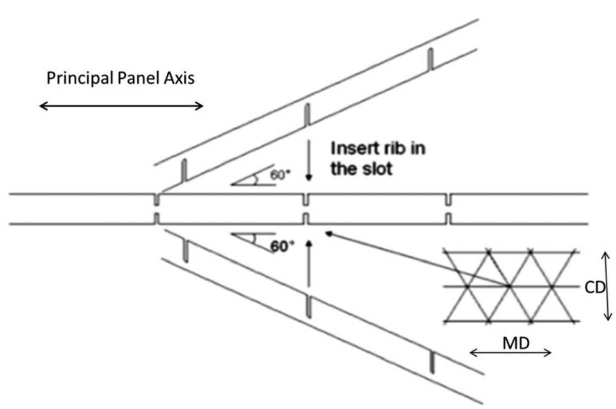

FIG. 2
The design of the tab/slot wood-based structural panel.

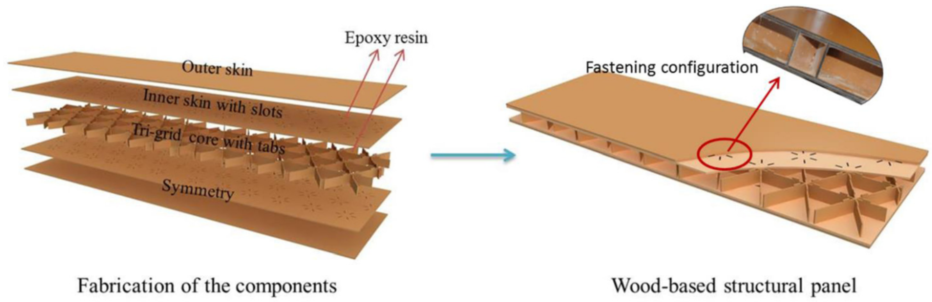

D695-10 [17], ASTM D638-14 [18], ASTM D5868-01(2014) [19], and ASTM D3846-08 [20]. NP610, Norplex-Micarta Inc. (Postville, IA), phenolic impregnated laminated paper was used for the core and faces of the structural panels. The laminated paper had orthogonal properties, namely the machine direction (MD) and the cross-machine direction (CD). The in-plane compression and tensile properties of the laminate papers along the MD and CD directions were obtained from in-house testing using the ASTM D695-10 [17] and ASTM D638-14 [18] standards, respectively. Poisson's ratios v_{xy} and v_{yx} were also obtained from the tensile tests by measuring both axial and transverse strains using biaxial extensometers. The in-plane shear properties of laminated paper were obtained from in-house material testing using ASTM D3846-08 [20]. Epoxy from U.S. Composites (West Palm Beach, FL) was used to bond the laminated paper faces and the core of the structural panels together. The ratio of epoxy to hardener was 3:1. The shear strength of the epoxy was determined using the lap shear test based on ASTM D5868-01(2014) [19]. The average epoxy shear strength was 17.9 MPa between the laminated papers. The material properties of the individual components used in the structural panels are listed in **Table 1**.

Design and Construction of the Wood-Fiber-Based Structural Panels

The wood-fiber-based structural panels were constructed from a tri-axially fabricated core using laminate paper as linear ribs in each of three axes with an interlocked structure (**Fig. 1**). The core or linear rib height was 33.0 mm. The slots in the linear ribs were cut slightly oversized to accommodate the 60° angular orientation between the ribs when assembled. The slot spacing for all pieces was 117.3 mm, thus, creating an equilateral triangle. The thickness of the ribs was 2.36 mm. Two configurations were used to analyze the effect of alignment of the core with the MD or CD alignment of the laminated paper faces. In order to enhance panel stability and avoid early failure due to weak interface between faces and core, a new fastening configuration of tabs and slots was applied to the ribs and faces and combined with the adhesive in order to obtain a better interfacial stress transfer into the core for the wood-fiber-based structural panels. The tabs on the interlocked triangular structural core were inserted into the slots on the top faces and bottom faces after the epoxy resin was poured on the faces. An additional laminated paper face was bonded on top of the slotted faces. Initial testing had shown the face stress capacity was reduced due to the slots in the faces that had reduced the cross-sectional area, so the added layer was to improve stress transfer to the entire face. The tab/slot fastening configuration was assumed as a fixed joint that modified the boundary condition to improve mechanical performance of either compression buckling in the face or shear in the core. The tab length on the ribs was 19.1 mm, the spacing distance between each tab was 38.1 mm, and each tri-grid repeatable element had six pairs of tabs and slots in both the face and core interfaces of the panel. The slot on the face was 20.3 mm in length and 2.54 mm in width, which was a little larger than the tab size in order to facilitate assembly (**Fig. 2**). All these components were cut using digitally controlled machines. Epoxy was used to bond the interfaces between the core and the inside face layers. Two additional panels were

TABLE 1 The material properties of components used in the composite structural panel.

Materials	Density (kg/m3)	Compressive Strength MD (MPa)	Compressive Strength CD (MPa)	Tensile Strength MD (MPa)	Tensile Strength CD (MPa)	In-Plane Shear Strength (MPa)	MOE MD (GPa)	MOE CD (GPa)	In-Plane Shear Modulus (GPa)	Poisson Ratios MD[a]	Poisson Ratios CD[b]
Laminated paper	1387	195.1	168.7	173.9	118.6	77.3	11.6	8.3	3.4	0.36	0.22
Epoxy resin	1101	105.9	—	31.0	—	17.9	1.4	—	—	0.42	—

[a]MD: machine direction.
[b]CD: cross-machine direction.

TABLE 2 The configuration and dimensions of the four structural panels used for the third point bending tests.

Panel	Panel size, l by w by t (mm)	Fastening Configuration	Rib Fiber Direction	Skin Thickness (mm)
1	1117.6 by 266.7 by 37.7	No tab and slot	MD	2.5
2	1117.6 by 266.7 by 37.8	Tab and slot	MD	2.6
3	1117.6 by 266.7 by 43.3	Tab and slot	MD	5.3
4	1117.6 by 266.7 by 43.0	Tab and slot	CD	5.2

fabricated for testing by adding an outer face layer to each side on top of the slotted faces. The nominal thickness of both the inside and outside face layers was 2.36 mm. Before applying epoxy resin, all laminate paper face surfaces were first prepared by lightly sanding on the glue side, and then the epoxy resin was spread on the faces for fabrication.

Table 2 shows the configuration and dimensions of the four wood-fiber-based structural panels tested for this study. One replicate for each type of wood-fiber-based structural panel was manufactured partly due to the cost associated with the production of these large panels and partly due to the reasonable repeatability. Panel 1 was made from a laminated paper tri-grid core in MD and faces without tabs or slots and was used as a control for Panel 2. Panel 2 was made from the same core and face structure as Panel 1 but with the tabs and slots. Panel 3 had the same main configuration as Panel 2; however, it had an additional laminate paper on top of the outer face layer. Panel 4 was made from the laminated paper tri-grid core in CD, with the rest of the components the same as Panel 3.

Third Point Load Bending Test

The four structural panels listed in **Table 2** were subjected to third point load bending according to ASTM C393/C393M-11e1 [21]. The structural panels were constructed and cut so that the ribs were centrally located to include three centrally located linear ribs. The spacing of the linear ribs was 101.6 mm. The span of the simple supported panel was 914 mm as shown in **Fig. 3(*a*)**. The width of the panel was 267 mm. The thicknesses of the panels ranged from 37.7 to 43.3 mm. Detailed dimensions for the four panels investigated are given in **Table 2**. Five linear variable differential transformers (LVDTs) were used for measuring the bending deflection at positions of 1/6, 1/3, 1/2, 2/3, and 5/6 span. The test setup is shown in **Fig. 3(*b*)**. Two types of strain gages including normal strain sensor CEA-06-250UN-350 and shear strain sensor CEA-06-187UV-350 were from Micro-Measurements Inc. M-Bond 200 adhesive from Micro-Measurements Inc. was used to bond strain gages to the panels after preparing localized surfaces on the panels. The specific positions of strain gage installations are shown in **Fig. 4**. In this test, 6 normal strain gages were attached to the mid-span section, including the outside top face (Gage 4), inside top face (Gage 1), upper linear rib in the core (Gage 5), lower linear rib in the core (Gage 6), inside bottom face (Gage 2), and outside bottom face (Gage 3), to measure the normal strain distribution and define the position of maximum normal strain. Another two normal strain Gages 7 and 8 were attached to measure the cross rib in the same section of the core, which was used to compare the relative positions by normal strain (Gage 5 and Gage 6) on complete linear ribs. Two shear strain gages were attached on a complete linear rib in mid-span (Gage 9) and in the shear zone (Gage 12), respectively. Another two shear strain gages were attached on the same section but on cross ribs (Gage 10 and Gage 11). The strain gage measurement program was built using LabVIEW. Twelve signal conditioners were connected to a 300-kN Instron 5587 test instrument to record the strain gage data. The 6 mm/min head load speed was used in the test.

FIG. 3 The set-ups for the third point bending test of the structural panel.

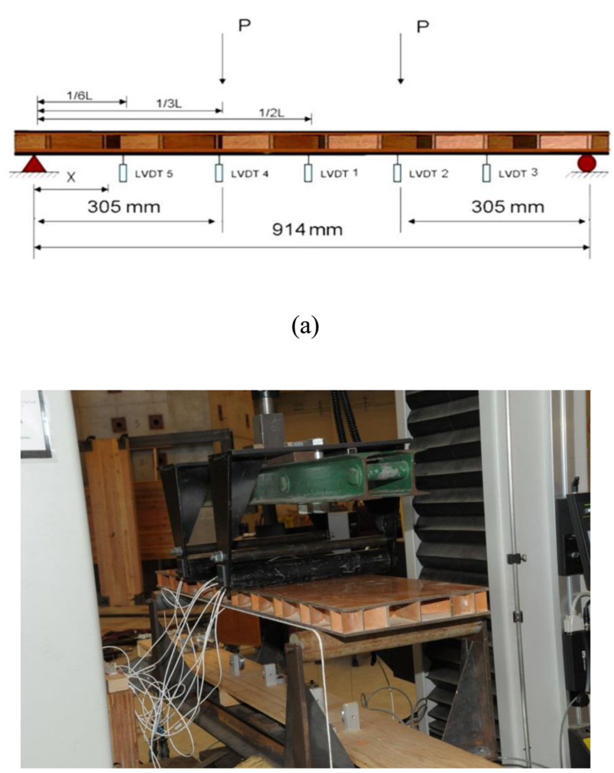

(a)

(b)

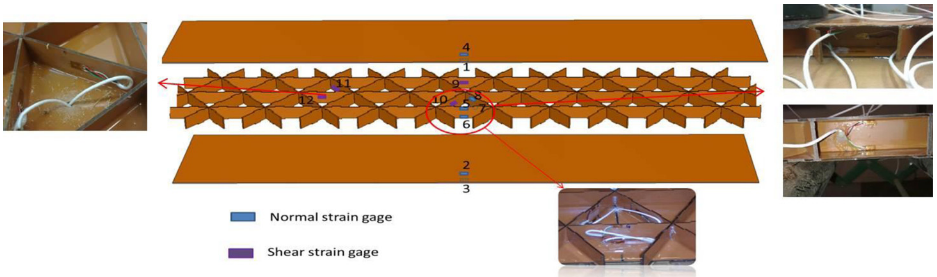

FIG. 4 The positions for the strain gages within the structural panel.

Discussion

PANEL BENDING CURVE AND FAILURE MODE

Figure 5(*a*) shows the typical plot of bending load versus mid-span deflection for structural Panels 1, 2, 3, and 4. Their bending failure loads were 11.5, 5.2, 18.4, and 21.8 kN, respectively. The panels began to make pinging noises around 5 kN and ended around 11 kN. Micro-cracking of the glue most likely caused this sound. Peak loads for thick Panels 3 and 4 with a two-layer face on each side were significantly higher than Panels 1 and 2 that had only a one-layer face on each side. The failure load for Panel 4, with CD core, was 15.6 % higher than that of Panel 3, which had linear ribs aligned with the panel. We believe that the fiber direction of the off-axis ribs has higher shear strength; thus, the shear capacity of the CD core is stronger than that of the MD core. Additionally, the failure load for Panel 3 with thick faces was 37.5 % and 72 % higher than that of Panel 1, which had a thinner face without a tabs or slots configuration, and that of Panel 2 with a tabs and slots configuration, respectively. This factor is likely because Panel 3 had two times the face thickness of Panels 1 and 2. Panel 2 had a lower failure load than Panel 1 because the slots in the faces reduced the actual bending cross-sectional area.

FIG. 5 The bending curves and failure modes of the four wood-based structural panels with different configuration.

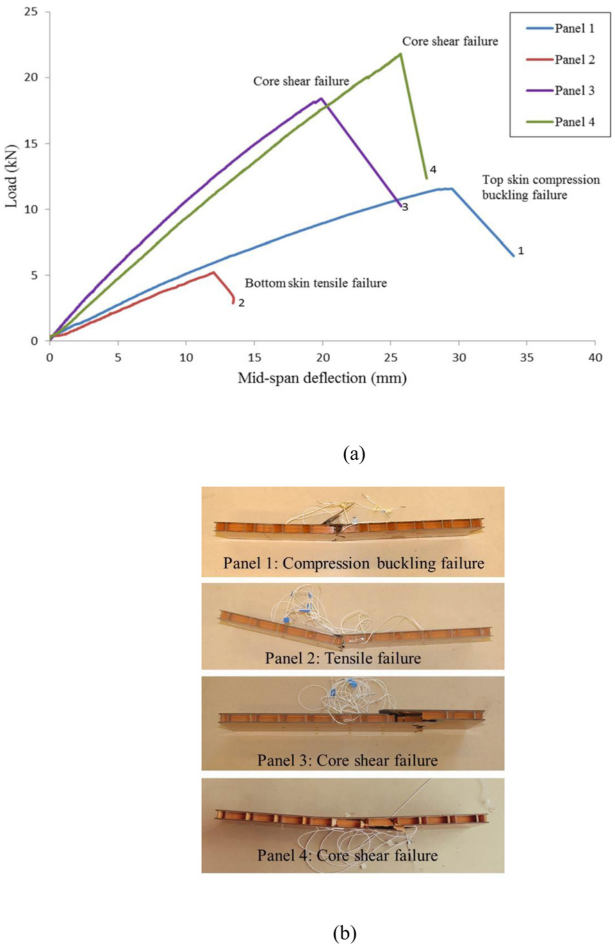

The bending failure modes for each panel are shown in **Fig. 5(*b*)**. Panel 1 exhibited compression buckling failures on the top face between load heads. We assumed core thickness had no vertical geometric change during the test, and the displacement of comparative compression buckling can be obtained from the displacement of load heads minus LVDT displacement in the same section. Panel 1 had a 2.5 mm comparative compression buckling on the top face at the loading point which represented 6.7 % of the panel thickness. Panel 2, with the new fastening configuration, only buckled 1.6 mm on the top face. Panels 3 and 4, with thicker faces, both buckled 1.75 mm. This was due to thicker faces having higher stiffness to resist buckling over an effective core. Panel 2 stiffness and load-carrying capacity were lower than those of Panel 1 due to a bottom face tensile failure as shown in **Fig. 5(*b*)**. This was primarily due to the lower ultimate strength of the bottom face. Thus, the additional face layer bonded to the surface of the slotted faces should help to avoid premature failure of the face/core interface. Nevertheless, Panel 2 displacement of relative vertical buckling was 36 % less than that for Panel 1 at the same loading conditions. The tab and slot configuration at the face/core interface acted as a clamped boundary that had better performance for resisting buckling. Panels 3 and 4 had the same tab and slot configuration and core dimensions except for the orientation of

FIG. 6 Load versus max normal strains for the faces in the mid-span section for the four panels.

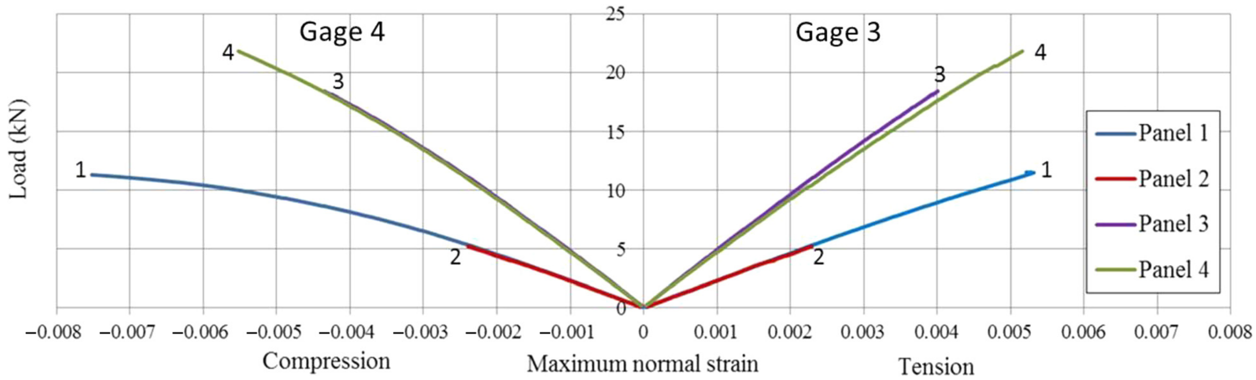

the tri-grid core. The failure modes of Panels 3 and 4 were similar, which had a core shear failure. The thickness of the faces for Panels 3 and 4 provided an increase in relative strength for the current tri-grid core, even for the stronger core that was aligned with CD. In this test, there were no premature peel failures by the initial bonding defect. Comparing Panels 1, 2, 3, and 4, we conclude that the stiffness and strength of wood-fiber-based structural panels significantly increases with face thickness combined with an effective structural core and vice versa. Both core shear failure and face failure either on compression or on tensile were the main failure modes for the panels with the tab and slots only. The observations show the fastening configuration design with epoxy resin in the face/core interface and additional outside faces may improve overall panel stability.

PANEL NORMAL STRAINS

Maximum Normal Strains on the Faces

Figure 6 plots the bending load versus maximum normal strain of both compression and tension in the mid-span section of each panel. The positive strains were tensile strain obtained from Strain Gage 3 at the bottom of each panel, and the negative strain curves were compression strain obtained from Strain Gage 4 at the top of each panel. The curves for Panels 1 and 2 have a similar trend; however, they have different maximum normal strains on both tension and compression due to the premature face failure for Panel 2 that occurred at the slots. Panel 2 maximum load was lower because of premature adhesive failure in tension in the slots causing the shear stress concentration at the bottom interface. Failure occurred suddenly due to the reduced face cross-sectional area. The cross-sectional area of the slotted faces of Panel 2 was 42.9 % less than that of the solid faces without slots as on Panel 1. As a result, the peak bending load of Panel 2 decreased by 54.7 % compared with the load of Panel 1. This can be explained based on the simple bending equation where the moment of inertia decreased due to the lower cross-sectional area, subsequently increasing the stress in the face of Panel 2. Compared with Panels 3 and 4, this indicates that the mechanical direction of the structural core made from orthotropic laminated paper had no noticeable effect on

FIG. 7 Load versus normal strains in the mid-span section of the longitudinal rib and cross rib. The solid lines represent the load and strain in the linear rib of each panel and the dashed lines represent the load and strain measured in the cross ribs of each panel.

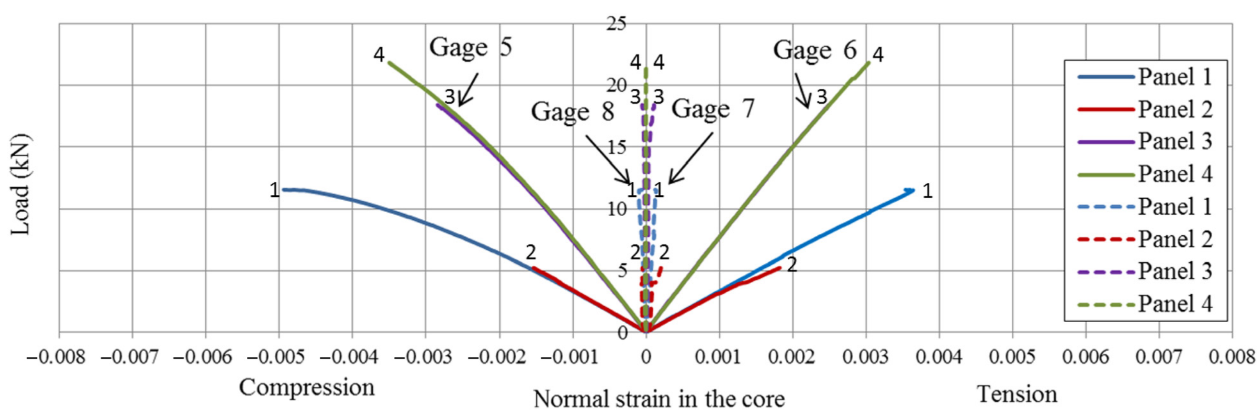

the normal strain, and the curves of load versus maximum normal strain are similar. However, panel thickness significantly influenced the normal strain distributions in the bending test according to a comparison of Panels 1 and 2 and Panels 3 and 4, which had different face thicknesses but the same dimensional height and spacing for the core. The normal face strains were lower in Panels 3 and 4 than the normal strains in Panels 1 and 2 under the same bending load due to the larger moment of inertia.

Maximum Normal Strains in the Core

Figure 7 plots load versus normal strain on both longitudinal and cross ribs of the structural core in the mid-span section of each panel. The positive curves are tensile strains measured via Strain Gages 6 and 7 for each panel on the lower ribs close to the bottom face. The negative curves are compression strains by Strain Gages 5 and 8 for each panel on the upper ribs close to the top faces. Solid lines are shown for Strain Gages 5 and 6 that measured strains in the complete linear rib. The dashed lines are shown for Strain Gages 7 and 8 that measured strains for the off-axis cross rib. Results yield a solid curve for each panel showing that normal strains in core for either compression or tension are smaller than the resulting maximum normal strains on the faces shown in **Fig. 6** that were due to normal stresses. The panels with thin faces also exhibited slight compression buckling in the core such as shown for Panel 1 as evident with the nonlinear effects of the load versus strain curves (**Fig. 6**). According to the moment of inertia of the panel, the faces had 90 % more contribution in bending than the structural core; therefore, the normal stress failure should occur first in the faces before they occur in the core, which was consistent with test results. Comparing the solid curve of longitudinal ribs to the dash curve of cross ribs demonstrates that cross ribs only minimally shared any stress during bending because of their predominant cross-direction orientation. Nevertheless, it is thought that the cross ribs of tri-grid core provide additional stiffness to the whole structure for plate applications with full side supports.

FIG. 8 The normal stress distributions in the mid-span section of each panel.

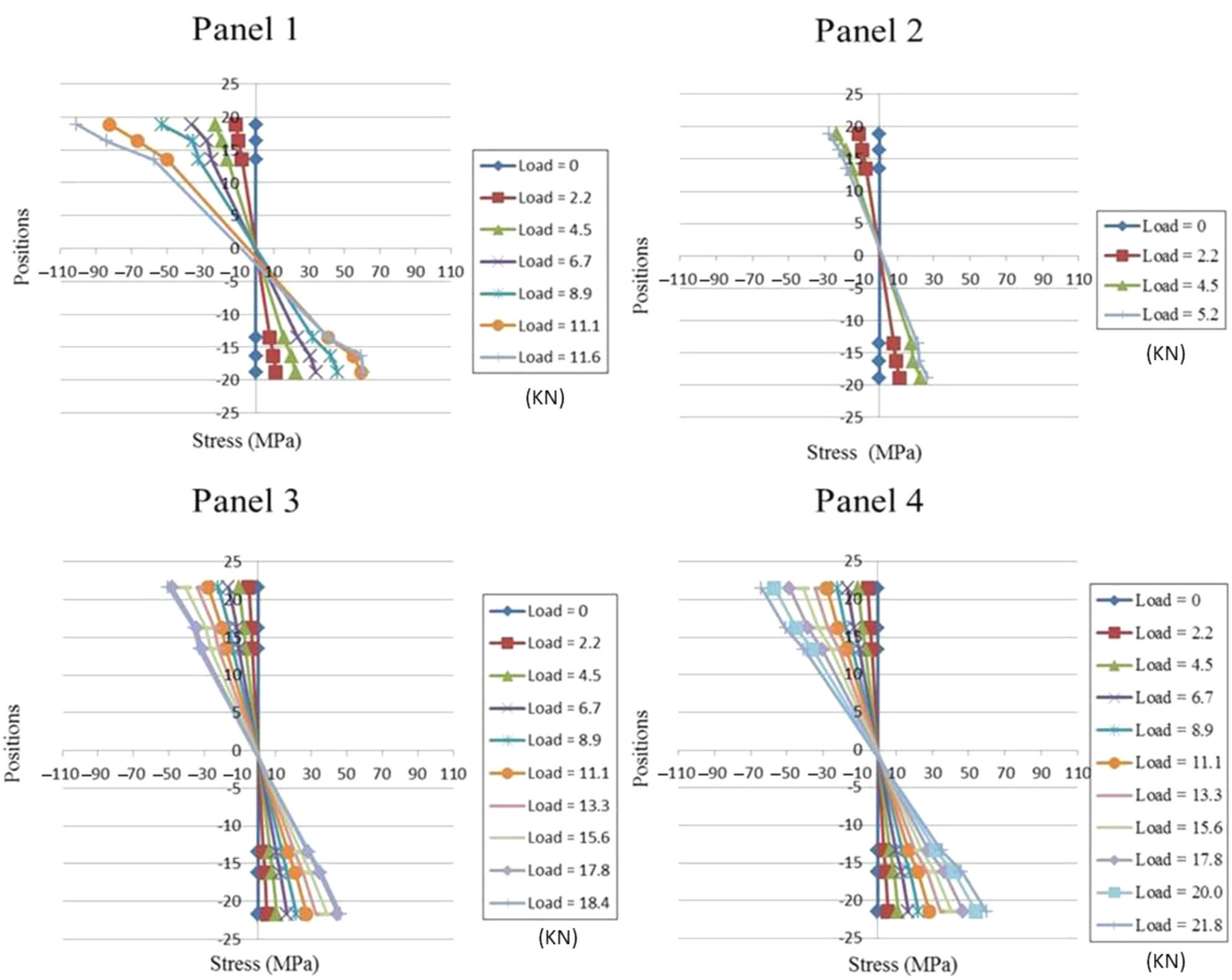

Normal Stress Distributions in the Mid-Span Section

Figure 8 plots normal stress distributions in the mid-span section of each panel by Strain Gages 4, 1, 5, 6, 2, and 3, which are attached from the top face to the bottom face under different load conditions. The vertical axis in the coordinate shows strain gage positions along with the panel thickness. The geometrical neutral axis of the panels is zero in the plot and the horizontal axis shows either (positive) tensile stress or (negative) compression stress. Panel 1 displays compression stress and tensile stress increasing as load increased up to 4.5 kN, and then the neutral axis begins to shift to a lower position as buckling begins to occur. Compression stress on the top face occurs in a nonlinear fashion and develops additional buckling deformation until the failure load. Tension stress on the bottom face increased linearly compared with the top face. Normal stress observed in the rib was not uniform, as load increased because the rib displayed a small amount of buckling on top. Therefore, we conclude that Panel 1 failed primarily due to compression buckling on the top face. It was also noticed that the neutral axis shifted down as evident with the increase shear stress starting from the faces and continuing into the core. Panel 2 core stress had similar initial stress behavior until brittle failure occurred between the slotted faces. Additional outside faces were applied to Panels 3 and 4. The tab into the slot configuration provided additional stability for the rib (prevention of buckling) and, thus, helped to increase stress transfer between the core and faces. The additional area from the tabs inserted into the slots increased the stability of the ribs compared with only an epoxy-bonded face/core interface. Panels 3 and 4 both show similar trends of normal stress transfer, but the maximum stress of Panel 4 was about 10 % higher. This was because the core for panel 4 had the MD properties of the laminated paper oriented across the rib with the CD properties aligned along the length of the ribs. This cross direction would have increased the shear stiffness of the resulting core material. The CD direction allowed for increased core shear transfer as evident in **Fig. 5(*a*)** with higher load capacity for Panel 4. The normal faces stress for either Panels 3 or 4 did not reach the maximum materials properties (**Table 1**) at failure load due to weakness in the core or core shear failure. The differences of the core orientation had only a slight effect on the normal stress distributions and final load-carrying capacity. However, the thickness and material mechanical properties of the faces are the primary factors that affected the normal stress distributions of the panels.

PANEL SHEAR STRAINS

Panel Shear Strains in the Core of the Shear Zone

Figure 9 plots the bending load versus shear strains in the panel's shear zone (between the load point and edge support) for each panel for both the linear rib and a cross rib. The solid curves measure shear strains in the linear rib using Gage 12, and the dashed curves measure shear strains in the cross rib using Gage 11. The results indicate the shear strain in the longitudinal rib was approximately 50 % larger than shear strains in the cross rib. These results are consistent with the theoretical transformation of cosine 60° between the linear rib and cross rib. We can define the relationship of shear strain between the linear rib and cross rib in terms of cosine transformation function with related angle of the ribs. In **Fig. 9**, the shear strains in the ribs of both Panels 1 and 2 were obviously less due to the failure in the faces than for the shear strains for Panels 3 and 4, where failure occurred in the core. The CD material property alignment ribs in Panel 4 provided improved shear load capacity for the core resulting in higher maximum load than the

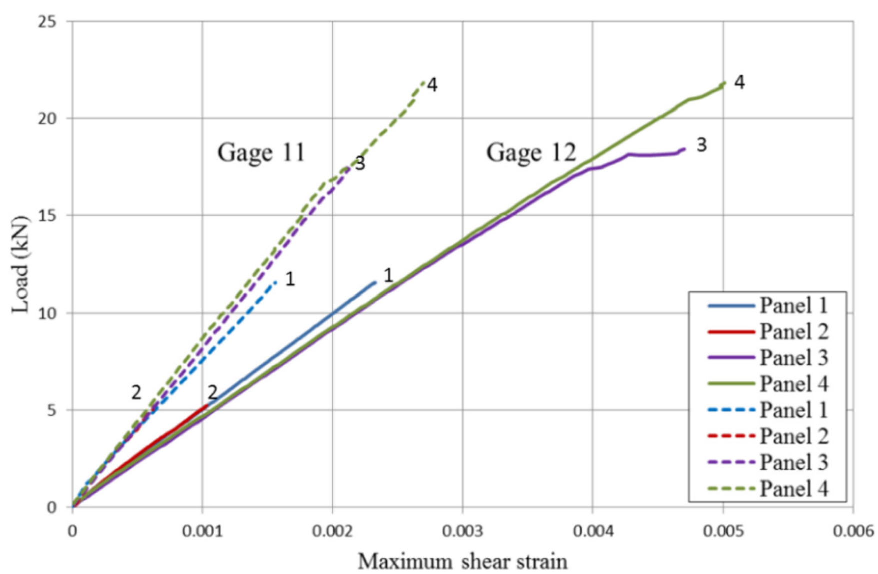

FIG. 9

Load versus shear strains in the core in the shear zone. The solid lines represent the load and strain in the linear rib of each panel and the dashed lines represent the load and strain measured in the cross ribs of each panel.

FIG. 10

Load versus shear strains in the core at mid-span positions. The solid lines represent the load and strain in the linear rib of each panel and the dashed lines represent the load and strain measured in the cross ribs of each panel.

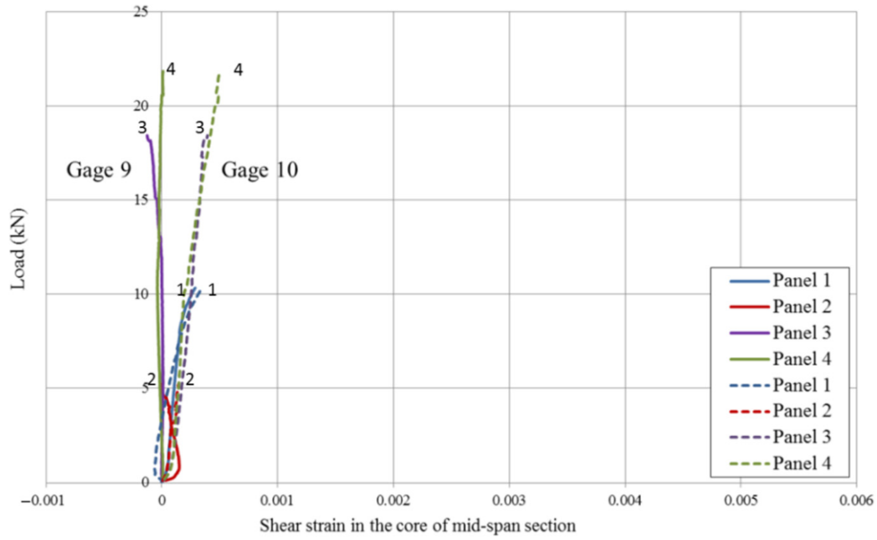

MD property alignment for the ribs of Panel 3. The CD fiber alignment in the rib perpendicular to the shear stress allowed for an increase in shear load across the ribs as well as within the tab. The shear strains increased with increasing load, and the maximum shear strain of Panel 4 reached 0.005 at 21.8 kN. The failure modes in **Fig. 5(*b*)** and strain distribution data for each panel reveal that Panel 1 and 2 had normal stress failure on the faces and Panel 3 and 4 were shear failures in the core. Therefore, the configuration of the panels appears to drive the primary critical failure modes for the wood-fiber-based structural panels.

Panel Shear Strains in the Core in the Mid-Span

Figure 10 plots shear strains in the mid-span section of the core of each panel. The solid curves for each panel were obtained from Gage 9 and measured strain for the linear rib while the dash curves for each panel were obtained from Gage 10 that measured strains for the cross ribs. The results illustrate the trends of each solid or dash curve changing irregularly, which are 10 times lower than results of the shear zone strains in **Fig. 9**. Based on the simple beam shear force diagram, there is a no shear zone between the two load legs, so we can assume equal shear in this zone is caused by noise. Therefore, the shear in this zone between the two load legs can be ignored in the design.

Conclusion

The third point load bending test of the panels with different face and core configurations exhibited significantly different bending behavior and strain characteristics measured by strain gages at several locations. The core shear failure and face failure either in compression or in tensile were two critical failure modes of the panels for the bending test. The failure modes were controlled by either the specific stiffness of the core/face or the structural configuration for the panels. The panel thickness also significantly influenced the strain distributions in the bending test, and the tab and slots configuration could improve the bonding stability in the core/face interface by these observations. For Panels 1 and 2, the normal stress failure occurred on the faces. The moment of inertia for Panel 2 is decided by the reduced section that illustrates the drop in peak load compared with Panel 1. For thicker Panels 3 and 4, the shear strain dominantly controlled the shear failure in the core, and the maximum shear stress occurred in the linear ribs in the shear zone, which was approximately twice as large as the shear strains in the cross rib in terms of the theoretical angle transformation. Either linear ribs or cross ribs in the mid-section of the core had little strain shown by the strain gages due to the no-shear zone between the two legs. For future study, the improved efficiency of the wood-fiber-based structural panels could be optimized based on ultimate normal strain in the face and ultimate shear strain in the core.

ACKNOWLEDGMENTS

This work is supported by the USDA Forest Products Laboratory. The authors gratefully acknowledge the support of Sara Fishwild, James Bridwell, Marshall Begel, Dave Simpson, and Marc Joyal of the EMRSL group for mechanical testing and Neil Gribbins for editorial assistance.

References

[1] Davalos, J. F., Qiao, P. Z., Xu, X. F., Robinson, J., and Barth, K. E., "Modeling and Characterization of Fiber-Reinforced Plastic Honeycomb Sandwich Panels for Highway Bridge Applications," *Compos. Struct.*, Vol. 52, Nos. 3–4, 2001, pp. 441–452.

[2] Li, J. H., Hunt, J. F., Cai, Z. Y., and Zhou, X. Y., "Bending Analyses for 3D Engineered Structural Panels Made From Laminated Paper and Carbon Fabric," *Compos. Part B: Eng.*, Vol. 53, 2013, pp. 17–24.
[3] Sharaf, T. and Fam, A., "Experimental Investigation of Large Scale Cladding Sandwich Panels Under Out-of-Plane Transverse Loading for Building Applications," *J. Compos. Constr.*, Vol. 15, No. 3, 2011, pp. 422–430.
[4] Vasiliev, V. V., Barynin, V. A., and Rasin, A. F., "Anisogrid Lattice Structures—Survey of Development and Application," *Compos. Struct.*, Vol. 54, Nos. 2–3, 2001, pp. 361–370.
[5] Wei, X., Tran, P., Vaucorbeil, A. D., Ramaswamy, R. B., Latourte, F., and Espinosa, H. D., "Three-Dimensional Numerical Modeling of Composite Panels Subjected to Underwater Blast," *J. Mech. Phys. Solids*, Vol. 61, No. 6, 2013, pp. 1319–1336.
[6] Allen, H. G., *Analysis and Design of Structural Sandwich Panels*, Pergamon Press, Oxford, UK, 1969.
[7] Fan, H. L., Zeng, T., Fang, D.-N., and Yang, W., "Mechanics of Advanced Fiber Reinforced Lattice Composites," *Acta. Mech. Sin.*, Vol. 26, No. 6, 2010, pp. 825–835.
[8] Jadhav, P., Mantena, P. R., and Gibson, R. F., "Energy Absorption and Damage Evaluation of Grid Stiffened Composite Panels Under Transverse Loading," *Compos. Part B: Eng.*, Vol. 37, Nos. 2–3, 2005, pp. 191–199.
[9] Fan, H. L., Yang, W., and Chao, Z. M., "Microwave Absorbing Composite Lattice Grids," *Compos. Sci. Technol.*, Vol. 67, Nos. 15–16, 2007, pp. 3472–3479.
[10] Evans, A. G., Hutchinson, J. W., Fleck, N. A., Ashby, M. F., and Wadley, H. N. G., "The Topology Design of Multifunctional Cellular Metals," *Prog. Mater. Sci.*, Vol. 46, No. 3, 2001, pp. 309–327.
[11] Chen, H. J. and Tsai, S. W., "Analysis and Optimum Design of Composite Grid Structures," *J. Compos. Mater.*, Vol. 30, No. 4, 1996, pp. 503–534.
[12] Fan, H. L., Meng, F. H., and Yang, W., "Sandwich Panels With Kagome Lattice Cores Reinforced by Carbon Fibers," *Compos. Struct.*, Vol. 81, No. 4, 2007, pp. 533–539.
[13] Huybrechts, S. M., Meink, T. E., Wegner, P. M., and Ganley, J. M., "Manufacturing Theory for Advanced Grid Stiffened Structures," *Compos. Part A: Appl. Sci. Manuf.*, Vol. 33, No. 2, 2002, pp. 155–161.
[14] Tsai, S. W., Liu, K. S., and Manne, P. M., "Manufacture and Design of Composite Grids," *Mater. Construct.*, Vol. 47, 1997, pp. 59–71.
[15] Han, D. Y. and Tsai, S. W., "Interlocked Composite Grids Design and Manufacturing," *J. Compos. Mater.*, Vol. 37, No. 4, 2003, pp. 287–316.
[16] Li, J. H., Hunt, J. F., Gong, S. Q., and Cai, Z. Y., "High Strength Wood-Based Sandwich Panels Reinforced With Fiberglass and Foam," *BioResources*, Vol. 9, No. 2, 2014, pp. 1898–1913.
[17] ASTM D695-10: Standard Test Method for Compressive Properties of Rigid Plastics, ASTM International, West Conshohocken, PA, 2010, www.astm.org.
[18] ASTM D638-14: Standard Test Method for Tensile Properties of Plastics, ASTM International, West Conshohocken, PA, 2014, www.astm.org.
[19] ASTM. D5868-01 (2014): Standard Test Method for Lap Shear Adhesion for Fiber Reinforced Plastic (FRP) Bonding, ASTM International, West Conshohocken, PA, 2014, www.astm.org.
[20] ASTM D3846-08: Standard Test Method for In-Plane Shear Strength of Reinforced Plastics, ASTM International, West Conshohocken, PA, 2008, www.astm.org.
[21] ASTM C393/C393M-11e1: Standard Test Method for Core Shear Properties of Sandwich Constructions by Beam Flexure, ASTM International, West Conshohocken, PA, 2011, www.astm.org.